EUROPEAN ORGANIZATION FOR NUCLEAR RESEARCH

CERN–PPE/95–53

21 April 1995

B^* Production in Z Decays

DELPHI Collaboration

Abstract

The decay $B^* \to B\gamma$ has been observed with the DELPHI detector at LEP, where the B^* meson is produced in Z boson decays. The combination of inclusively reconstructed B mesons with well-measured converted photons yields a measurement of the flavour-averaged $B^* - B$ mass difference of 45.5 ± 0.3 (stat.) $\pm$ 0.8 (syst.) MeV/c^2. 95% confidence level upper limits at 6 MeV/c^2 are placed on both the isospin (i.e. B^+-B^0) and the B_s-B_{ud} splitting of the mass difference. The production ratio of B^* to B mesons in Z decays is measured to be 0.72 ± 0.03 (stat.) $\pm$0.06 (syst.). Limits on the production cross-section of other hypothetical excited B hadron states decaying radiatively are established. The differential B^* cross section has been measured to be in good agreement with the average b fragmentation, yielding an average fractional B^* energy of $\langle x_E \rangle$ =0.695 $\pm$ 0.009 (stat.) $\pm$ 0.013 (syst.) . From the decay angular distribution the relative contribution of longitudinal B^* polarisation states is measured to be $\sigma_L/(\sigma_L + \sigma_T) = 0.32 \pm 0.04$ (stat.) $\pm$0.03 (syst.).

(To be submitted to Zeit f. Physik C)

P.Abreu[21], W.Adam[50], T.Adye[37], E.Agasi[31], I.Ajinenko[42], R.Aleksan[39], G.D.Alekseev[16], P.P.Allport[22], S.Almehed[24], S.J.Alvsvaag[4], U.Amaldi[9], S.Amato[47], A.Andreazza[28], M.L.Andrieux[14], P.Antilogus[25], W-D.Apel[17], Y.Arnoud[39], B.Åsman[44], J-E.Augustin[19], A.Augustinus[31], P.Baillon[9], P.Bambade[19], F.Barao[21], R.Barate[14], D.Y.Bardin[16], G.J.Barker[35], A.Baroncelli[40], O.Barring[24], J.A.Barrio[26], W.Bartl[50], M.J.Bates[37], M.Battaglia[15], M.Baubillier[23], J.Baudot[39], K-H.Becks[52], M.Begalli[6], P.Beilliere[8], Yu.Belokopytov[9], A.C.Benvenuti[5], M.Berggren[41], D.Bertrand[2], F.Bianchi[45], M.Bigi[45], M.S.Bilenky[16], P.Billoir[23], D.Bloch[10], M.Blume[52], S.Blyth[35], V.Bocci[38], T.Bolognese[39], M.Bonesini[28], W.Bonivento[28], P.S.L.Booth[22], G.Borisov[42], C.Bosio[40], S.Bosworth[35], O.Botner[48], B.Bouquet[19], C.Bourdarios[9], T.J.V.Bowcock[22], M.Bozzo[13], P.Branchini[40], K.D.Brand[36], R.A.Brenner[15], C.Bricman[2], L.Brillault[23], R.C.A.Brown[9], P.Bruckman[18], J-M.Brunet[8], L.Bugge[33], T.Buran[33], A.Buys[9], M.Caccia[28], M.Calvi[28], A.J.Camacho Rozas[41], T.Camporesi[9], V.Canale[38], M.Canepa[13], K.Cankocak[44], F.Cao[2], F.Carena[9], P.Carrilho[47], L.Carroll[22], C.Caso[13], M.V.Castillo Gimenez[49], A.Cattai[9], F.R.Cavallo[5], L.Cerrito[38], V.Chabaud[9], Ph.Charpentier[9], L.Chaussard[25], J.Chauveau[23], P.Checchia[36], G.A.Chelkov[16], R.Chierici[45], P.Chliapnikov[42], P.Chochula[7], V.Chorowicz[9], V.Cindro[43], P.Collins[9], J.L.Contreras[19], R.Contri[13], E.Cortina[49], G.Cosme[19], F.Cossutti[46], H.B.Crawley[1], D.Crennell[37], G.Crosetti[13], J.Cuevas Maestro[34], S.Czellar[15], E.Dahl-Jensen[29], J.Dahm[52], B.Dalmagne[19], M.Dam[33], G.Damgaard[29], A.Daum[17], P.D.Dauncey[37], M.Davenport[9], W.Da Silva[23], C.Defoix[8], G.Della Ricca[46], P.Delpierre[27], N.Demaria[35], A.De Angelis[9], H.De Boeck[2], W.De Boer[17], S.De Brabandere[2], C.De Clercq[2], C.De La Vaissiere[23], B.De Lotto[46], A.De Min[28], L.De Paula[47], C.De Saint-Jean[39], H.Dijkstra[9], L.Di Ciaccio[38], F.Djama[10], J.Dolbeau[8], M.Donszelmann[9], K.Doroba[51], M.Dracos[10], J.Drees[52], K.-A.Drees[52], M.Dris[32], Y.Dufour[8], F.Dupont[14], D.Edsall[1], R.Ehret[17], G.Eigen[4], T.Ekelof[48], G.Ekspong[44], M.Elsing[52], J-P.Engel[10], N.Ershaidat[23], B.Erzen[43], M.Espirito Santo[21], E.Falk[24], D.Fassouliotis[32], M.Feindt[9], A.Ferrer[49], T.A.Filippas[32], A.Firestone[1], H.Foeth[9], E.Fokitis[32], F.Fontanelli[13], F.Formenti[9], B.Franek[37], P.Frenkiel[8], D.C.Fries[17], A.G.Frodesen[4], R.Fruhwirth[50], F.Fulda-Quenzer[19], H.Furstenau[9], J.Fuster[49], A.Galloni[22], D.Gamba[45], M.Gandelman[6], C.Garcia[49], J.Garcia[41], C.Gaspar[9], U.Gasparini[36], Ph.Gavillet[9], E.N.Gazis[32], D.Gele[10], J-P.Gerber[10], L.Gerdyukov[42], M.Gibbs[22], D.Gillespie[9], R.Gokieli[51], B.Golob[43], G.Gopal[37], L.Gorn[1], M.Gorski[51], Yu.Gouz[42], V.Gracco[13], E.Graziani[40], G.Grosdidier[19], P.Gunnarsson[44], M.Gunther[48], J.Guy[37], U.Haedinger[17], F.Hahn[52], M.Hahn[17], S.Hahn[52], Z.Hajduk[18], A.Hallgren[48], K.Hamacher[52], W.Hao[31], F.J.Harris[35], V.Hedberg[24], R.Henriques[21], J.J.Hernandez[49], P.Herquet[2], H.Herr[9], T.L.Hessing[9], E.Higon[49], H.J.Hilke[9], T.S.Hill[1], S-O.Holmgren[44], P.J.Holt[35], D.Holthuizen[31], M.Houlden[22], J.Hrubec[50], K.Huet[2], K.Hultqvist[44], P.Ioannou[3], J.N.Jackson[22], R.Jacobsson[44], P.Jalocha[18], R.Janik[7], G.Jarlskog[24], P.Jarry[39], B.Jean-Marie[19], E.K.Johansson[44], L.Jonsson[24], P.Jonsson[24], C.Joram[9], P.Juillot[10], M.Kaiser[17], G.Kalmus[37], F.Kapusta[23], M.Karlsson[44], E.Karvelas[11], S.Katsanevas[3], E.C.Katsoufis[32], R.Keranen[15], B.A.Khomenko[16], N.N.Khovanski[16], B.King[22], N.J.Kjaer[29], H.Klein[9], A.Klovning[4], P.Kluit[31], J.H.Koehne[17], B.Koene[31], P.Kokkinias[11], M.Koratzinos[9], K.Korcyl[18], V.Kostioukhine[42], C.Kourkoumelis[3], O.Kouznetsov[13], P.-H.Kramer[52], M.Krammer[50], C.Kreuter[17], J.Krolikowski[51], I.Kronkvist[24], Z.Krumstein[16], W.Krupinski[18], P.Kubinec[7], W.Kucewicz[18], K.Kurvinen[15], C.Lacasta[49], I.Laktineh[25], S.Lamblot[23], J.W.Lamsa[1], L.Lanceri[46], D.W.Lane[1], P.Langefeld[52], V.Lapin[42], I.Last[22], J-P.Laugier[39], R.Lauhakangas[15], G.Leder[50], F.Ledroit[14], V.Lefebure[2], C.K.Legan[1], R.Leitner[30], Y.Lemoigne[39], J.Lemonne[2], G.Lenzen[52], V.Lepeltier[19], T.Lesiak[36], D.Liko[50], R.Lindner[52], A.Lipniacka[19], I.Lippi[36], B.Loerstad[24], M.Lokajicek[12], J.G.Loken[35], J.M.Lopez[41], A.Lopez-Fernandez[9], M.A.Lopez Aguera[41], D.Loukas[11], P.Lutz[39], L.Lyons[35], J.MacNaughton[50], G.Maehlum[17], A.Maio[21], V.Malychev[16], J.Marco[41], B.Marechal[47], M.Margoni[36], J-C.Marin[9], C.Mariotti[40], A.Markou[11], T.Maron[52], C.Martinez-Rivero[41], F.Martinez-Vidal[49], S.Marti i Garcia[49], F.Matorras[41], C.Matteuzzi[28], G.Matthiae[38], M.Mazzucato[36], M.Mc Cubbin[9], R.Mc Kay[1], R.Mc Nulty[22], J.Medbo[48], C.Meroni[28], W.T.Meyer[1], M.Michelotto[36], E.Migliore[45], L.Mirabito[25], W.A.Mitaroff[50], U.Mjoernmark[24], T.Moa[44], R.Moeller[29], K.Moenig[9], M.R.Monge[13], P.Morettini[13], H.Mueller[17], L.M.Mundim[6], W.J.Murray[37], B.Muryn[18], G.Myatt[35], F.Naraghi[14], F.L.Navarria[5], S.Navas[49], P.Negri[28], S.Nemecek[12], W.Neumann[52], N.Neumeister[50], R.Nicolaidou[3], B.S.Nielsen[29], M.Nieuwenhuizen[31], V.Nikolaenko[10], P.Niss[44], A.Nomerotski[36], A.Normand[35], W.Oberschulte-Beckmann[17], V.Obraztsov[42], A.G.Olshevski[16], R.Orava[15], K.Osterberg[15], A.Ouraou[39], P.Paganini[19], M.Paganoni[28], P.Pages[10], H.Palka[18], Th.D.Papadopoulou[32], L.Pape[9], C.Parkes[35], F.Parodi[13], A.Passeri[40], M.Pegoraro[36], L.Peralta[21], H.Pernegger[50], M.Pernicka[50], A.Perrotta[5], C.Petridou[46], A.Petrolini[13], H.T.Phillips[37], G.Piana[13], F.Pierre[39], M.Pimenta[21], S.Plaszczynski[19], O.Podobrin[17], M.E.Pol[6], G.Polok[18], P.Poropat[46], V.Pozdniakov[16], M.Prest[46], P.Privitera[38], N.Pukhaeva[16], A.Pullia[28], D.Radojicic[35], S.Ragazzi[28], H.Rahmani[32], J.Rames[12], P.N.Ratoff[20], A.L.Read[33], M.Reale[52], P.Rebecchi[19], N.G.Redaelli[28], M.Regler[50], D.Reid[9], P.B.Renton[35], L.K.Resvanis[3], F.Richard[19], J.Richardson[22], J.Ridky[12], G.Rinaudo[45], I.Ripp[39], A.Romero[45], I.Roncagliolo[13], P.Ronchese[36], V.Ronjin[42], L.Roos[14], E.I.Rosenberg[1], E.Rosso[9], P.Roudeau[19], T.Rovelli[5], W.Ruckstuhl[31], V.Ruhlmann-Kleider[39], A.Ruiz[41], H.Saarikko[15], Y.Sacquin[39], A.Sadovsky[16], G.Sajot[14], J.Salt[49], J.Sanchez[26], M.Sannino[13], H.Schneider[17], M.A.E.Schyns[52], G.Sciolla[45], F.Scuri[46], Y.Sedykh[16], A.M.Segar[35], A.Seitz[17], R.Sekulin[37], R.C.Shellard[6], I.Siccama[31], P.Siegrist[39], S.Simonetti[39], F.Simonetto[36], A.N.Sisakian[16], B.Sitar[7], T.B.Skaali[33], G.Smadja[25], N.Smirnov[42], O.Smirnova[16], G.R.Smith[37], R.Sosnowski[51], D.Souza-Santos[6], T.Spassov[21], E.Spiriti[40], S.Squarcia[13], H.Staeck[52], C.Stanescu[40], S.Stapnes[33], I.Stavitski[36], K.Stepaniak[51], F.Stichelbaut[9], A.Stocchi[19], J.Strauss[50], R.Strub[10], B.Stugu[4], M.Szczekowski[51], M.Szeptycka[51], T.Tabarelli[28], J.P.Tavernet[23], O.Tchikilev[42], A.Tilquin[27], J.Timmermans[31], L.G.Tkatchev[16], T.Todorov[10], D.Z.Toet[31], A.Tomaradze[2], B.Tome[21], L.Tortora[40], G.Transtromer[24], D.Treille[9], W.Trischuk[9],

G.Tristram[8], A.Trombini[19], C.Troncon[28], A.Tsirou[9], M-L.Turluer[39], I.A.Tyapkin[16], M.Tyndel[37], S.Tzamarias[22], B.Ueberschaer[52], S.Ueberschaer[52], O.Ullaland[9], V.Uvarov[42], G.Valenti[5], E.Vallazza[9], C.Vander Velde[2], G.W.Van Apeldoorn[31], P.Van Dam[31], W.K.Van Doninck[2], J.Van Eldik[31], N.Vassilopoulos[35], G.Vegni[28], L.Ventura[36], W.Venus[37], F.Verbeure[2], M.Verlato[36], L.S.Vertogradov[16], D.Vilanova[39], P.Vincent[25], L.Vitale[46], E.Vlasov[42], A.S.Vodopyanov[16], V.Vrba[12], H.Wahlen[52], C.Walck[44], F.Waldner[46], A.Wehr[52], M.Weierstall[52], P.Weilhammer[9], A.M.Wetherell[9], D.Wicke[52], J.H.Wickens[2], M.Wielers[17], G.R.Wilkinson[35], W.S.C.Williams[35], M.Winter[10], M.Witek[9], G.Wormser[19], K.Woschnagg[48], K.Yip[35], O.Yushchenko[42], F.Zach[25], C.Zacharatou[24], A.Zaitsev[42], A.Zalewska[18], P.Zalewski[51], D.Zavrtanik[43], E.Zevgolatakos[11], N.I.Zimin[16], M.Zito[39], D.Zontar[43], R.Zuberi[35], G.C.Zucchelli[44], G.Zumerle[36]

[1] Ames Laboratory and Department of Physics, Iowa State University, Ames IA 50011, USA
[2] Physics Department, Univ. Instelling Antwerpen, Universiteitsplein 1, B-2610 Wilrijk, Belgium
and IIHE, ULB-VUB, Pleinlaan 2, B-1050 Brussels, Belgium
and Faculté des Sciences, Univ. de l'Etat Mons, Av. Maistriau 19, B-7000 Mons, Belgium
[3] Physics Laboratory, University of Athens, Solonos Str. 104, GR-10680 Athens, Greece
[4] Department of Physics, University of Bergen, Allégaten 55, N-5007 Bergen, Norway
[5] Dipartimento di Fisica, Università di Bologna and INFN, Via Irnerio 46, I-40126 Bologna, Italy
[6] Centro Brasileiro de Pesquisas Físicas, rua Xavier Sigaud 150, RJ-22290 Rio de Janeiro, Brazil
and Depto. de Física, Pont. Univ. Católica, C.P. 38071 RJ-22453 Rio de Janeiro, Brazil
and Inst. de Física, Univ. Estadual do Rio de Janeiro, rua São Francisco Xavier 524, Rio de Janeiro, Brazil
[7] Comenius University, Faculty of Mathematics and Physics, Mlynska Dolina, SK-84215 Bratislava, Slovakia
[8] Collège de France, Lab. de Physique Corpusculaire, IN2P3-CNRS, F-75231 Paris Cedex 05, France
[9] CERN, CH-1211 Geneva 23, Switzerland
[10] Centre de Recherche Nucléaire, IN2P3 - CNRS/ULP - BP20, F-67037 Strasbourg Cedex, France
[11] Institute of Nuclear Physics, N.C.S.R. Demokritos, P.O. Box 60228, GR-15310 Athens, Greece
[12] FZU, Inst. of Physics of the C.A.S. High Energy Physics Division, Na Slovance 2, 180 40, Praha 8, Czech Republic
[13] Dipartimento di Fisica, Università di Genova and INFN, Via Dodecaneso 33, I-16146 Genova, Italy
[14] Institut des Sciences Nucléaires, IN2P3-CNRS, Université de Grenoble 1, F-38026 Grenoble Cedex, France
[15] Research Institute for High Energy Physics, SEFT, P.O. Box 9, FIN-00014 Helsinki, Finland
[16] Joint Institute for Nuclear Research, Dubna, Head Post Office, P.O. Box 79, 101 000 Moscow, Russian Federation
[17] Institut für Experimentelle Kernphysik, Universität Karlsruhe, Postfach 6980, D-76128 Karlsruhe, Germany
[18] High Energy Physics Laboratory, Institute of Nuclear Physics, Ul. Kawiory 26a, PL-30055 Krakow 30, Poland
[19] Université de Paris-Sud, Lab. de l'Accélérateur Linéaire, IN2P3-CNRS, Bat 200, F-91405 Orsay Cedex, France
[20] School of Physics and Materials, University of Lancaster, Lancaster LA1 4YB, UK
[21] LIP, IST, FCUL - Av. Elias Garcia, 14-1^{o}, P-1000 Lisboa Codex, Portugal
[22] Department of Physics, University of Liverpool, P.O. Box 147, Liverpool L69 3BX, UK
[23] LPNHE, IN2P3-CNRS, Universités Paris VI et VII, Tour 33 (RdC), 4 place Jussieu, F-75252 Paris Cedex 05, France
[24] Department of Physics, University of Lund, Sölvegatan 14, S-22363 Lund, Sweden
[25] Université Claude Bernard de Lyon, IPNL, IN2P3-CNRS, F-69622 Villeurbanne Cedex, France
[26] Universidad Complutense, Avda. Complutense s/n, E-28040 Madrid, Spain
[27] Univ. d'Aix - Marseille II - CPP, IN2P3-CNRS, F-13288 Marseille Cedex 09, France
[28] Dipartimento di Fisica, Università di Milano and INFN, Via Celoria 16, I-20133 Milan, Italy
[29] Niels Bohr Institute, Blegdamsvej 17, DK-2100 Copenhagen 0, Denmark
[30] NC, Nuclear Centre of MFF, Charles University, Areal MFF, V Holesovickach 2, 180 00, Praha 8, Czech Republic
[31] NIKHEF-H, Postbus 41882, NL-1009 DB Amsterdam, The Netherlands
[32] National Technical University, Physics Department, Zografou Campus, GR-15773 Athens, Greece
[33] Physics Department, University of Oslo, Blindern, N-1000 Oslo 3, Norway
[34] Dpto. Fisica, Univ. Oviedo, C/P. Pérez Casas, S/N-33006 Oviedo, Spain
[35] Department of Physics, University of Oxford, Keble Road, Oxford OX1 3RH, UK
[36] Dipartimento di Fisica, Università di Padova and INFN, Via Marzolo 8, I-35131 Padua, Italy
[37] Rutherford Appleton Laboratory, Chilton, Didcot OX11 OQX, UK
[38] Dipartimento di Fisica, Università di Roma II and INFN, Tor Vergata, I-00173 Rome, Italy
[39] Centre d'Etude de Saclay, DSM/DAPNIA, F-91191 Gif-sur-Yvette Cedex, France
[40] Istituto Superiore di Sanità, Ist. Naz. di Fisica Nucl. (INFN), Viale Regina Elena 299, I-00161 Rome, Italy
[41] C.E.A.F.M., C.S.I.C. - Univ. Cantabria, Avda. los Castros, S/N-39006 Santander, Spain, (CICYT-AEN93-0832)
[42] Inst. for High Energy Physics, Serpukov P.O. Box 35, Protvino, (Moscow Region), Russian Federation
[43] J. Stefan Institute and Department of Physics, University of Ljubljana, Jamova 39, SI-61000 Ljubljana, Slovenia
[44] Fysikum, Stockholm University, Box 6730, S-113 85 Stockholm, Sweden
[45] Dipartimento di Fisica Sperimentale, Università di Torino and INFN, Via P. Giuria 1, I-10125 Turin, Italy
[46] Dipartimento di Fisica, Università di Trieste and INFN, Via A. Valerio 2, I-34127 Trieste, Italy
and Istituto di Fisica, Università di Udine, I-33100 Udine, Italy
[47] Univ. Federal do Rio de Janeiro, C.P. 68528 Cidade Univ., Ilha do Fundão BR-21945-970 Rio de Janeiro, Brazil
[48] Department of Radiation Sciences, University of Uppsala, P.O. Box 535, S-751 21 Uppsala, Sweden
[49] IFIC, Valencia-CSIC, and D.F.A.M.N., U. de Valencia, Avda. Dr. Moliner 50, E-46100 Burjassot (Valencia), Spain
[50] Institut für Hochenergiephysik, Österr. Akad. d. Wissensch., Nikolsdorfergasse 18, A-1050 Vienna, Austria
[51] Inst. Nuclear Studies and University of Warsaw, Ul. Hoza 69, PL-00681 Warsaw, Poland
[52] Fachbereich Physik, University of Wuppertal, Postfach 100 127, D-42097 Wuppertal 1, Germany

1 Introduction

In e^+e^- collisions at the Large Electron-Positron (LEP) collider at CERN, with centre-of-mass energies close to the Z^0 mass of 91.2 GeV, the copious production of $b\bar{b}$ events offers a laboratory for B meson spectroscopy. The b quarks produced in the decay $Z \to b\bar{b}$ receive a significant Lorentz boost that is largely transmitted to the B hadrons in the hadronisation process. The mass difference between the pseudoscalar B meson and its vector partner B^* is about 46 MeV/c^2 [1–5], in agreement with the prediction of the quark model extrapolation from the D meson sector. Due to this small mass difference, all strong decays are kinematically forbidden and the electromagnetic $M1$ transition, $B^* \to B\gamma$, is the dominant decay mode. At LEP energies these decays result in a photon spectrum that extends up to just 800 MeV.

A substantial fraction of $Z \to b\bar{b}$ decays are expected to lead to B^* meson production, as recently confirmed by the L3 Collaboration [4]. An estimate of the relative abundance of B^* to B mesons can be made based on their inherent spin structure differences since their mass splitting is small compared with the average B energy. The number of spin degrees of freedom for a particle of spin J is $(2J+1)$. Under the assumption of uniform population of these states, the production ratio should be 3:1 for vector to pseudoscalar mesons, and the ratio of transverse (T) to longitudinal (L) B^* polarisation states should be 2:1, independent of the b-quark polarisation. These ratios are also predicted by heavy quark effective theory (HQET) [6].

The DELPHI detector can study B^* decays by using inclusively reconstructed B mesons with well-measured converted photons to detect any $B\gamma$ signal. The high resolution vertex detector allows DELPHI to tag $b\bar{b}$ events efficiently. In the analysis that follows, an enriched sample of $b\bar{b}$ events from the 1991 to 1994 LEP runs is used. Measurements will be presented for the flavour-averaged B-meson hyperfine splitting, and that of B_s-mesons, a limit on the hyperfine splitting differences between charged and neutral B mesons, the B^*/B production cross section ratio, limits on the abundance of radiative decays of other b-hadrons up to the pion production threshold, the energy differential B^* cross-section, and a polarisation analysis of the B^* photon angular distribution in the B^* rest frame.

2 The DELPHI detector and event selection

DELPHI is a 4π detector with emphasis on precise vertex information, particle identification, three dimensional reconstruction and high granularity. A complete description can be found in reference [7]. The detectors most relevant to this study are the tracking chambers (Vertex Detector, Inner Detector, Time Projection Chamber and Outer Detector) and the barrel electromagnetic calorimeter (High-density Projection Chamber).

The DELPHI vertex detector consists of three concentric cylindrical shells of Si-strip detectors at radii of 6.3, 9 and 11 cm parallel to the beampipe for precision reconstruction near the interaction region. The algorithm that is used to enhance the $b\bar{b}$ content relies on good vertex measurements. Therefore the analysis is restricted to the barrel region ($45° < \theta < 135°$, θ denoting the polar angle with respect to the beam axis), where there is complete vertex detector coverage.

Inclusive reconstruction of the B momentum relies on DELPHI's tracking capabilities. The combined tracking in the barrel region has a momentum resolution as a function of momentum, p, of $\sigma(p)/p = 0.0011 \cdot p$ for muon pairs, where p is in GeV/c. Photons and π^0's that are reconstructed by the High-density Projection Chamber (HPC) have a

resolution, σ, as a function of energy, of $\sigma(E)/E \approx \sqrt{0.26^2/E + 0.046^2}$ (E in GeV) and an angular resolution of around ± 2 mrad in azimuthal and polar angles ϕ and θ.

To calculate efficiencies, backgrounds, biases and resolutions for the current analysis, the DELPHI simulation package DELSIM [8] is employed; this uses the JETSET 7.3 model generator [9] with parameter adjustments from previous QCD studies [10]. In addition, the $B^* - B$ mass difference in the JETSET generator was fixed to the current PDG world average [5] in order to avoid errors in acceptance effects due to an incorrect B^* photon energy spectrum.

Using standard barrel hadronic Z event cuts [11] around 2.33 million events are selected from the 1991 to 1994 LEP runs. About twice as many simulation events were available. The bases of the technique [12] used to create a sample enriched in $b\bar{b}$ events are the lifetime and decay multiplicity differences between the B meson and lighter D mesons. The B meson is nearly three times heavier than the $D^{\pm}$ meson with a lifetime that is 50 percent longer. Furthermore, the energy spectrum of the B meson is generally harder than that for primary D mesons, and the B decays into a D meson most of the time. These features result in a distribution of impact parameters that is characteristically larger in B meson events than in events without B mesons. The probability is calculated for each event that all the well-measured tracks originate from a single vertex compatible with the beam spot. Selecting events where this probability is less than 1% results in an efficiency of $(52 \pm 3)\%$ and a purity of $(80 \pm 4)\%$ for $b\bar{b}$ events. This beauty-enhanced sample consists of 333,738 events.

3 Inclusive B meson reconstruction

Inclusive B meson momentum reconstruction uses an algorithm based on measured momenta and angles only. This works well for B mesons due to their large mass and their hard fragmentation function. Simulation studies show that the rapidity $y = 0.5 \cdot \log((E + p_z)/(E - p_z))$ of B mesons along the event thrust axis should be strongly peaked at $y = \pm 2.4$, with some spread towards lower $|y|$ due to hard gluon radiation (see figure 1a). Another observation is that the B meson decay products should have a Gaussian distribution in rapidity space with a width of about 0.8 units. In b-events the fragmentation process mainly generates particles at lower rapidities, and their distribution can be described by two Gaussians of width 1.05 units, centered at ± 1.03. The model-dependence of these distributions has been analyzed by comparing the predictions of JETSET 7.4 [9] and HERWIG 5.8 [13] (with the JETSET decays), both with default parameters. In general these two predictions differ by less than 10% at any y in the inclusive y distribution from fragmentation, and by less than 4% in the distribution from B decays.

Detector acceptance and resolution effects have only a small influence on these distributions, the most important being that the loss of low energy particles leads to a suppression of the population at low $|y|$. The inclusive rapidity distributions for DELPHI data and simulation are shown in figure 1b. Excellent agreement is observed for both charged and neutral particles.

The events are divided into two hemispheres defined by the thrust axis. The rapidity of each reconstructed charged (assuming the pion mass) and neutral particle (assuming the photon mass) with respect to the thrust axis is calculated. Particles outside a central rapidity window of ± 1.5 units are considered to be B meson decay products. The 4-momenta of these particles are added together in each hemisphere to arrive at a B meson energy estimate E_y for each side of the event.

Given the inclusive nature of this reconstruction technique there are events that are not well reconstructed. However, most of these poorly reconstructed events are removed by requiring that:

1. a minimum energy of 20 GeV is reconstructed for the B candidate in the rapidity-gathering algorithm;
2. the reconstructed mass lies within ± 2.5 GeV/c^2 of the average reconstructed B meson mass;
3. the ratio of hemisphere energy, E_{hem}, to beam energy, E_{beam}, lies in the range $0.6 < x_h = E_{hem}/E_{beam} < 1.1$.

Enforcing these requirements results in a loss of 26 % of B decays.

Studies using simulation showed that a strong correlation exists between the generated B meson energy, E_{Btrue}, and the initial estimate E_y from the rapidity-gathering algorithm described above. There is a further correlation between the energy residuals $\Delta E = E_y - E_{Btrue}$ and the reconstructed B meson mass m_y, which is approximately linear in m_y. Also a correlation between ΔE and the ratio of the energy seen in the hemisphere to the beam energy $x_h = E_{hem}/E_{beam}$ is observed, reflecting global inefficiencies and neutrino losses. Since the mass and hemisphere energy dependences are not independent, a correction technique taking into account their correlations is applied.

A correction function is determined using simulated events in the following way. After applying all cuts, the simulated data are divided into several samples according to the measured ratio x_h. For each of these classes the energy residual ΔE is plotted as function of the reconstructed mass m_y. The median values of ΔE in each bin of m_y are calculated, and their m_y dependence fitted by a second order polynomial, $\Delta E(m_y; x_h\text{-bin}) = a + b \cdot (m_y - \langle m_y \rangle) + c \cdot (m_y - \langle m_y \rangle)^2$. The three coefficients in the fit, a, b and c, in each x_h class are then plotted as function of x_h and their dependence fitted using second order polynomials, $a(x_h) = a_1 + a_2 \cdot x_h + a_3 \cdot x_h^2$, and similarly for $b(x_h)$ and $c(x_h)$. Thus one obtains a smooth correction function describing the mean dependence on m_y and the hemisphere energy, characterized by 9 parameters $a_i, b_i, c_i, i = 1, 3$. Finally, a small "bias correction" is applied for the mean remaining energy residual as a function of the corrected energy, as determined from simulation.

The attainable precision of this inclusive technique depends on the cuts on the b-tagging probability, event shape variables (thrust, number of jets) and the B quality cuts. For the standard cuts described above the energy precision is 7% for 75% of the B mesons, the remainder constituting a non-Gaussian tail towards higher energies. The angular resolution in θ and ϕ can be parameterized as double Gaussians with widths of 15 mrad for 60% of the data and 38 mrad for the remaining 40%.

The good agreement between data and Monte Carlo simulation for the reconstructed B mass m_y and corrected fractional B energy x_E distributions is shown in figures 1c and 1d.

4 Converted photon reconstruction

The energy spectrum for the photons from $B^* \to B\gamma$ decays is not in a favorable region for reconstruction in the HPC. The low-energy acceptance of the HPC would limit the range of accessible photon energies, and the detected photons are reconstructed with an inherent resolution that goes as $1/\sqrt{E}$. In order to overcome these difficulties, this analysis is restricted to photons converted to e^+e^- in material before the TPC.

Photon conversions in front of the TPC are reconstructed by an algorithm that examines tracks reconstructed in the TPC. A search is made along each TPC track for points where the tangent of its trajectory points directly to the beam spot in the $R\phi$ projection. Under the assumption that the opening angle of the electron-positron pair is zero, this point represents a possible photon conversion point at radius R. All tracks which have a solution R that is more than one standard deviation away from the main vertex, as defined by the beam-spot, are considered to be conversion candidates. Since the radius of curvature increases with increasing energy, higher momentum tracks often have a solution R consistent with the primary vertex. The one standard deviation cut is necessary to keep background at a tolerable level, but it does limit the efficiency at high energies.

If two oppositely charged conversion candidates are found with compatible decay point parameters they are linked together to form one converted photon. The following selection criteria are imposed:

1. the reconstructed mean conversion radius (in the $r\phi$ plane) is below 34 cm;
2. at least one of the tracks has no associated point in front of the reconstructed mean conversion radius;
3. the ϕ difference between the two conversion points is at most 30 mrad;
4. the difference between the polar angles θ of the two tracks is at most 15 mrad.

For the pairs fulfilling these criteria a χ^2 is calculated in order to find the best combinations in cases where there are ambiguous associations. A constrained fit is then applied to the electron-positron pair candidate which forces a common conversion point with zero opening angle and collinearity between the momentum sum and the line from the beam spot to the conversion point. The energy of the conversion electrons is corrected for radiation losses by a small factor that depends on the amount of material between the conversion point and the entrance to the TPC. From Monte Carlo simulation the reconstruction precision of these converted photons with an acceptable χ^2 has been determined to be 1% in energy, 1.5 mrad in polar and azimuthal angles θ and ϕ, and 5 mm in conversion radius.

At very low energies the acceptance drops for asymmetric conversions since the TPC can only reconstruct electrons with a transverse momentum with respect to the beam above 50 MeV/c. In order to reconstruct these single electron conversions, photon conversion track candidates are only used if they have not been paired with another candidate. They are accepted as singles only when the following conditions are satisfied:

1. the conversion radius is between 22 and 33 cm;
2. the conversion point is at least 4 standard deviations away from the beam crossing (in the $r\phi$ plane);
3. no hits are measured in front of the reconstructed conversion point;
4. the z-coordinate of the conversion point and that from the angular extrapolation from the reconstructed primary vertex towards the conversion point must coincide within 1 cm.

After applying a mean correction for the unseen electron an energy resolution of approximately 10% is achieved. The single electron conversions represent 25% of all converted photons in the data and effectively lower the acceptance threshold from 250 MeV to 100 MeV.

This conversion reconstruction is also used for an analysis of the inclusive π^0 cross section [14]. The photon energy scale and angular resolutions can be monitored by comparing the π^0 peaks reconstructed by combining two converted photons in data and

simulation. Figure 2 shows good agreement in the π^0 peak position and width, which is observed globally and for different energy range selections. The fitted π^0 peak positions are 135.2 ± 0.2 MeV/c^2 in real data and 134.8 ± 0.2 MeV/c^2 in simulation, both in agreement with the PDG value 134.97 MeV/c^2. The remaining scale uncertainty on the converted photon energy is thus limited to 0.3%. The Gaussian widths of the signals are 4.7 ± 0.3 MeV/c^2 (data) and 4.4 ± 0.3 MeV/c^2 (simulation). The acceptance is calculated using the simulation sample. Photon energy and $\gamma\gamma$ invariant mass spectra using conversion pairs, single electron conversions and HPC photons, as well as the conversion radius distribution have been checked to be in general agreement with the simulation prediction. The low energy threshold is well and reliably modelled, since it is just determined by geometry: in order to be reconstructable in the TPC, a track must cross at least three pad rows. Remaining small differences (mainly due to wrong associations of noise hits in the vertex detectors) are corrected for.

5 Measurement of the mean $B^* - B$ mass difference

The mean mass difference between the vector and pseudoscalar B mesons can be measured by combining the reconstructed B four-momentum with the photon from the B^*, calculating the mass of the combination, and then subtracting the B mass value reconstructed in that event. Figure 3a shows the distribution of the mass difference between the B^* candidates and the reconstructed B mesons. The combinatorial background is mainly due to photons from π^0 decays that are combined with the reconstructed B meson. It is well described by the simulation prediction (dashed line). The cut-off of the combinatorial background at low ΔM is correlated to the photon energy threshold. On top of this background there is a clear signal due to $B^* \to B\gamma$ decays.

There are three kinematic variables involved in the determination of the mass difference, namely the magnitude of the B momentum, the photon energy, and the angle between the B meson and the photon. The mass difference can be expressed to a good approximation in terms of these kinematic variables as

$$\Delta M(B^* - B) = E_\gamma \gamma (1 - \beta \cos \Theta),$$

where E_γ is the photon energy in the lab frame, $\gamma = E_B/m_B$ is the B meson's Lorentz time dilation factor, $\beta = \sqrt{1 - 1/\gamma^2} \approx 1$ is the B meson velocity, and Θ is the angle between the B meson and the B^* photon. Each of the kinematic variables has an experimental resolution which contributes to the width of the peak, which is 6.6 MeV/c^2 when fitted with a single Gaussian. The B momentum resolution contributes approximately 3 MeV/c^2 to the measured width. The photon energy resolution contributes only around 2 MeV/c^2 (better for the reconstructed pairs, worse for single track reconstructions). The angular resolution between the B meson and the B^* photon dominates the width of the mass difference peak. The photon angular resolution can be neglected compared to the B meson angular resolution. The contribution to the measured width from the total angular resolution is about 4.0 MeV/c^2, as derived from the simulation. A much better parameterization of the peak is achieved using two Gaussians of equal area and widths of 4.5 MeV/c^2 and 10.1 MeV/c^2, with the broader contribution slightly shifted towards lower masses to describe the asymmetry in the tails.

The peak position in the data and simulation is stable against the division of events in bins of $x_E = E_B/E_{beam}$, in photon selection from one-track conversions or full reconstructions, and for different $b\bar{b}$ enrichment cuts. In all cases, the simulation describes both

the signal and background shapes well. For this reason, the simulation distributions have been used to fit the data. The advantage of this method is that only three fit parameters are required: the mass difference and the normalizations of the signal and background.

The simulation was produced with a $B^* - B$ mass difference of 46 MeV/c^2, but can be used to test different hyperfine splitting hypotheses. This is accomplished in the simulation by calculating the measurement residuals of the B energy, photon energy and opening angle on an event by event basis. New "true" values for the photon energy and the laboratory opening angle are calculated for a different mass difference, leaving the B momentum and the photon decay angle in the B^* rest frame fixed. Finally the measurement residuals are added back in. This effectively calculates the mass difference signal distribution (including the non-Gaussian tails) in each step of the fit. The data histogram is fitted using a sum of simulation background and manipulated simulation B^* signal histograms, both smoothed in order to reduce effects due to limited simulation statistics.

The result of this fit is a mass difference of 45.5 ± 0.3 (stat.) MeV/c^2.

A two-Gaussian fit to the peak in figure 3b leads to a central value of the narrow Gaussian which is lower by 0.5 MeV/c^2. This bias inherent in the inclusive reconstruction method is predicted by the Monte Carlo simulation, and is automatically accounted for in the fit procedure.

The main systematic uncertainty in the peak position comes from the B momentum reconstruction. Using different B energy correction procedures, varying cuts in wide ranges, and changing the fragmentation function and detector resolutions in reasonable limits, the systematic uncertainty on the mass difference due to the B momentum reconstruction is estimated to be 1.8%. Compared to this, the $\pm 0.3\%$ systematic uncertainty due to the photon energy calibration estimated using the results from the π^0 fit can be neglected. The resulting mass difference is thus

$$\Delta M(B^* - B) = 45.5 \pm 0.3\ (stat.)\ \pm 0.8\ (syst.)\ MeV/c^2.$$

This result agrees with the previous measurements of CUSB [1] (52 ± 2 (stat.) ± 4 (syst.) MeV/c^2), CUSB2 [2] (45.4 ± 1.0 MeV/c^2), and CLEO2 [3] (46.2 ± 0.3 (stat.) $\pm$ 0.8 (syst.) MeV/c^2) and L3 [4] (46.3 ± 1.9 (stat.) MeV/c^2).

In a second series of fits, the possibility of different hyperfine splitting values for the three different flavours of B mesons is examined. The simulated B meson sample is composed of B_u, B_d and B_s mesons in an approximate ratio of $3:3:1$. Based on a comparison of the signal width in data and simulation, an upper limit can be placed on the differences between the B meson flavour splitting within the peak. This is accomplished by using the peak manipulation procedure for the simulation described above, enforcing the ratio of the different B meson species, and allowing each flavour of B meson to have a variable hyperfine splitting value.

The evolution of the fit χ^2 as a function of the difference between the flavour-dependent hyperfine values is almost flat at small values and rises sharply beyond about 5 MeV/c^2 (the measurement resolution scale). In fact, the best fits are obtained including a small isospin splitting of 3.5 MeV/c^2. In these fits the $B_s^* - B^*$ mass difference was fixed at 45.5 MeV/c^2. From the χ^2 distribution the following upper limit is derived:

$$|\Delta M(B^{*+} - B^+) - \Delta M(B^{*0} - B^0)| < 6.0 \text{ MeV/c}^2 \text{ (at 95\% c.l.)} .$$

The present analysis is sensitive to any radiative decay of an excited b-hadron $X_b^* \to X_b\gamma$. This makes it possible to put limits on the corresponding production cross-section $\sigma(b \to X_b^*)$, where X_b^* denotes a state other than the B_{ud}^*. Figure 4 displays the

95% confidence level upper limits for the production rates of such hypothetical states as a function of the mass difference. In determining these limits the variation of the photon acceptance as a function of ΔM has been taken into account and no assumption has been made about the B^* cross-section.

To determine the $B_s^* - B_s$ mass difference an assumption has to be made about the B_s^* cross-section. Within the JETSET model this cross-section is determined by the strangeness suppression factor (1/3) and hence amounts to 1/7 of the total B^* cross-section. B_s^{**} production effectively lowers this rate since this meson cannot decay into $B_s\pi$ because of isospin conservation, leaving BK as the main decay mode. Recently experimental evidence for the transition $b \to B^{**}$ has been established, at a rate of $\approx 30\%$ [16,17]. Thus the ratio of B_s^* to all B^* mesons is expected to be 10 %.

From figure 4 it can be seen that the $B_s^* - B_s$ mass splitting must be close to that for non-strange b-mesons, as long as the B_s^* is produced in 4% or more of all b-jets. A recent compilation of heavy flavour baryon measurements [15] suggests that b-baryons are produced in $(10 \pm 4)\%$ of b-quark jets in Z decays. Subtracting the baryon contribution and using the B^*/B production rate determined later in this paper (0.72), the expected branching ratio is $B(b \to B_s^*)$ is 6.8 %, thus satisfying the requirement.

To obtain an upper limit for the B_s^*-B_s mass difference, the χ^2 evolution as a function of the B_s mass difference was investigated, fitting at each step the $B_{u,d}$ mass difference, signal and background normalisations, but fixing the B_s^*/B^* production cross-section ratio to the expected 10%. The fits have been repeated using B_s^*/B^* production ratios down to 5%. The fit χ^2 is quite flat around the main peak position, but then strongly rises. From this an upper limit can be established:

$$|\Delta M(B_s^* - B_s) - \Delta M(B_{ud}^* - B_{ud})| < 6.0 \text{ MeV/c}^2 \text{ (at 95\% c.l.)} .$$

This limit confirms the measurement from CUSB2 [2] ($\Delta M(B_s^* - B_s) = 47.0 \pm 2.6$ MeV/c^2), also based on indirect evidence for B_s^* production.

6 Measurement of the B^*/B production cross-section ratio

The fit described in the previous section yields the total number of B^*s reconstructed

$$N(B^*) = 3009 \pm 108\ (stat.)\ \pm 65\ (syst.) .$$

where the systematic error is based on the shapes used in the fitting procedure. Using the acceptance as determined from simulation, the ratio of B^* to b-quark cross-sections is

$$\sigma_{B^*}/\sigma_{b-quark} = 0.65 \pm 0.02\ (stat.)\ \pm 0.06\ (syst.)\ ,$$

where the systematic error includes a 2% uncertainty from the fitting procedure, a 7% uncertainty in the photon efficiency and a 5% uncertainty due to the $b\bar{b}$ purity. Making use of the measured fraction of $b\bar{b}$ events in hadronic Z decays [5] the number of B^* mesons per hadronic Z decays is

$$N_{B^*}/Z_{had} = 0.28 \pm 0.01\ (stat.)\ \pm 0.03\ (syst.)\ .$$

In order to extract the B^* to B cross-section ratio, the expected number of b-baryons needs to be subtracted from the number of b-jets in order to arrive at the total number

of b-mesons in the sample. Subtracting a $10 \pm 4\%$ b-baryon contribution [15], the cross-section ratio emerges as

$$\sigma_{B^*}/(\sigma_B + \sigma_{B^*}) = 0.72 \pm 0.03\ (stat.)\ \pm 0.06\ (syst.)\ .$$

Here σ_B is the primary B production rate, excluding feed-down from B^* decays. This result is in agreement with the result from L3 [4] (0.76 ± 0.08 (stat.) $\pm$ 0.06 (syst.)).

In the absence of B^{**} production, this ratio is simply equal to the parameter $V/(V+P)$ in the JETSET fragmentation model [9], where V and P are the production rates of primary vector and pseudoscalar B mesons. However, production of a sizeable amount of B^{**} mesons can alter the ratio of B^* to B mesons depending on the relative production and branching fractions into $B^*\pi$ and $B\pi$ of the four individual B^{**} spin-parity states. No measurements of the production rates of these spin-parity states exist, though, as mentioned in section 5, the total B^{**} rate has been measured [16,17]. A further complication arises from the way JETSET treats the production of the two 1^+ states: one is made from the P ($S = 0$) fraction, and the other, together with the 0^+ and the 2^+ states, from the V ($S = 1$) fraction. HQET however predicts the two 1^+ eigenstates to be $45°$ mixtures of $S = 0$ and $S = 1$. Different assumptions, such as relative $2^+ : 1^+ : 1^+ : 0^+$ production ratios between $1 : 1 : 1 : 1$ (state counting) and $5 : 3 : 3 : 1$ (spin counting) and 2^+ decay branching ratios into $B^*\pi$ from 25% to 50%, change the effective branching fraction of B^{**} to B^* only within the range 55% to 75%. Taking the measured B^{**}/b production fraction of $f^{**} = (30 \pm 5)\%$ and $Br(B^{**} \to B^*) = (65 \pm 10)\%$ this implies

$$\frac{V}{V+P} = \frac{1}{1-f^{**}}\left(\frac{\sigma_{B^*}}{\sigma_B + \sigma_{B^*}} - f^{**} \cdot Br(B^{**} \to B^*)\right) = 0.75 \pm 0.10,$$

where the error is calculated using quadratic addition of statistical and systematic errors of the single contributions.

7 Measurement of the B^* fragmentation function

In order to analyze the differential B^* cross-section, the data sample is divided into seven equally populated bins in $x_E = E_B/E_{beam}$, and the $B^* - B$ mass difference plot is fitted in each of these bins. An unfolding procedure is applied that uses the simulated B sample to generate the reconstructed energy spectrum $x_{E,rec}$ in each of five bins of true energy $x_{E,true}$; every event being weighted with the average photon acceptance as a function of true energy. A fit to the data histogram is performed using the five simulation histograms. The fit parameters determine the normalization coefficients of the simulation histograms such that the resulting histogram of the reconstructed energies best describes the data. In order to avoid spurious oscillations that are typical in such unfolding procedures [18], regularisation is enforced by adding to the χ^2 a term proportional to the curvature of the unfolding result, as follows:

$$\chi^2 \to \chi'^2 = \chi^2 + \tau \cdot \int |f''(x)|^2\, dx \approx \chi^2 + \tau \cdot \sum_{i=2}^{n-1} |f_{i-1} - 2 \cdot f_i + f_{i+1}|^2\ .$$

The regularisation parameter, τ, was chosen so as to minimize the condition number (i.e. the ratio of the largest to the smallest eigenvalue) of the correlation matrix ($\tau = 2.5$). Much smaller values lead to oscillating solutions and large negative correlations, whereas too large values lead to too flat solutions, too small errors and strong positive correlations. However, the results are stable in the τ range between 0.1 and 10.

The final differential cross-section as a function of the true energies is obtained by multiplying these relative deviations from the simulation prediction by the simulation input cross-section. The result is shown in figure 5. It has been checked that the result is independent of the fragmentation function used in the simulation by repeating the unfolding procedure with Monte Carlo events weighted as a function of x_{Etrue}.

The mean fractional energy of B^* mesons is determined from the unfolded x_E distribution in the following way. The JETSET 7.4 model with default parameters, but B^{**} meson production included at a level compatible with recent experimental findings [16,17], is used to determine the $x_E(B^*)$ distributions for various values of the Peterson fragmentation parameter ϵ_b. For all these distributions a χ^2 describing the deviation from the measured distribution (fig. 5) is calculated. Then a central value for ϵ_b and the error is determined from the functional dependence of χ^2 on ϵ_b. The prediction of the best fit is shown as curve in fig. 5. Finally, the ϵ_b values are translated into $\langle x_E \rangle$ using the JETSET model prediction. The result is:

$$\langle x_E \rangle = 0.695 \pm 0.009 \ (stat.) \ \pm 0.013 \ (syst.) \ .$$

The main systematic error comes from the 1.8 % uncertainty in the B energy correction procedure, and from model uncertainty in the extrapolation into the unmeasured low x_E range. The Peterson parameter found, $\epsilon_b = 0.0006 \pm 0.0001$, is harder to interpret than $\langle x_E \rangle$, since it is strongly correlated to the values of the parton shower cutoff Q_0 and of α_s used in the model, and different tunings of these parameters can imply a very different value for ϵ_b in order to achieve the same x_E distribution. In addition, not allowing B^{**} production in the JETSET 7.4 simulation, but otherwise using unchanged parameters for the comparison with the data results in a significantly softer Peterson fragmentation parameter ϵ_b of 0.0004 ± 0.0001.

The B^* differential cross-section is, within errors, compatible with the default JETSET model prediction, that the B^*/B ratio is independent of the B energy. The measured mean B^* energy is in agreement with the mean B energy $\langle x_E \rangle = 0.7030 \pm 0.0085$, determined from semileptonic B-decays using the DELPHI detector [19]. This latter quantity is expected to be about 0.7% lower than the mean fractional B^* energy.

8 B^* helicity analysis

Since B^* mesons are vector particles they can be described by the polarisation states ± 1 and 0 along their direction of flight. The two transverse (T) helicity states, ± 1, each lead to an angular distribution proportional to $(1 + \cos^2 \theta^*)/2$, where θ^* is the angle between the direction of flight of the B^* meson in the laboratory frame and the photon in the B^* rest frame. The longitudinal (L) helicity state, 0, leads to a $\sin^2 \theta^*$ distribution. If the helicity states are equally populated, i.e. $\sigma_T : \sigma_L = 2 : 1$, the photon angular distribution should be isotropic.

The Standard Model predicts a large polarisation for b-quarks (–0.94 for quarks and +0.94 for anti-quarks). If the b-quark polarisation is preserved in the hadronisation process and thus transferred to the B^* meson, a large asymmetry in the population of the $+1$ and -1 helicity states would result. Unfortunately, the two helicity states lead to the same angular distribution in the B^* rest frame and cannot be separated without knowledge of the photon helicity.

In order to determine the helicity structure of the B^* mesons, each B^* photon candidate is boosted to the B^* frame and the helicity angle, θ^*, is calculated. There is a strong correlation between the rest frame angle and the photon energy, backward decays

being lower in photon energy. There is essentially no acceptance for $\cos\theta^*$ below -0.5, so this region is ignored. The remaining range is divided into six bins in $\cos\theta^*$, which is reconstructed with a resolution of $\sigma(\cos\theta^*) = 0.15$. A single-parameter fit to the ΔM distribution is performed in each $\cos\theta^*$ bin, with the background normalisations held constant. Background and signal shapes are calculated with the measured mass and are taken from simulation. The fits are good in all bins. The results are shown as points in figure 6.

The helicity angle distribution is fitted with the angular decay distribution functions, with the two degrees of freedom being the relative strength of the longitudinal polarisation state and the overall normalization. The systematic error for this measurement is dominated by the uncertainty in the photon acceptance as a function of the helicity angle $\cos\theta^*$. The range between -0.5 and 0 is dominated by conversions reconstructed from a single electron. By analyzing conversion pairs and singles separately, the total uncertainty has been estimated to be 7%. The uncertainty in the energy dependence of the photon acceptance propagates into a 10% difference in the result of the fit. The relative longitudinal contribution is determined to be

$$\sigma_L/(\sigma_L + \sigma_T) = 0.32 \pm 0.04\ (stat.)\ \pm 0.03\ (syst.)\ .$$

The result of the fit is shown in figure 6.

9 Summary and conclusions

B^* decays have been identified from a peak in the $M(B+\gamma) - M(B)$ mass difference using an inclusive B reconstruction method and converted photons. The mean (averaged over B_u, B_d and B_s) mass difference has been measured to be 45.5 $\pm$ 0.3 (stat.) $\pm$ 0.8 (syst.) MeV/c^2. The measurement resolution sets an upper limit on the isospin-splitting of the mass difference $|\Delta M(B^{*+} - B^+) - \Delta M(B^{*0} - B^0)| < 6.0\,\mathrm{MeV/c^2}$ at the 95% confidence level.

Limits have been placed on the production cross-section of hypothetical excited B hadron states decaying radiatively. These limits in particular indicate that the B_s^* is contained within the global B^* peak, assuming B_s^* production rate is at least 4%. From this the B_s hyperfine splitting can be restricted to $|\Delta M(B_s^* - B_s) - \Delta M(B_{ud}^* - B_{ud})| < 6.0\,\mathrm{MeV/c^2}$ at the 95% confidence level.

The ratio of the number of B^* mesons to hadronic Z decays is 0.28 $\pm$ 0.01 (stat.) $\pm$ 0.03 (syst.) and that of B^* mesons to B mesons (i.e. whether B^* decay products or not) 0.72 $\pm$ 0.03 (stat.) $\pm$ 0.06 (syst.) Correcting for effects due to B^{**} production and decay, this corresponds to a vector to vector plus pseudoscalar ratio $V/(V+P) = 0.75 \pm 0.10$.

The fragmentation function of the B^* has been measured to be compatible with the average B hadron fragmentation function; the mean fractional B^* energy is determined to be $\langle x_E \rangle = 0.695 \pm 0.009$ (stat.) $\pm$0.013 (syst.).

A fit to the helicity angle distribution results in the ratio $\sigma_L/(\sigma_L + \sigma_T)$ =0.32 $\pm$ 0.04 (stat.) $\pm$ 0.03 (syst.) These measurements are compatible with the expectation of a simple spin counting picture with no vector suppression ($\sigma_{B^*}/\sigma_B = 0.75, \sigma_L/(\sigma_L + \sigma_T) = 0.33$), which is also predicted by HQET. The B system thus appears to be a much better approximation to the "Heavy Quark Limit" than the D system. However, this simple picture is complicated by the apparently large B^{**} production rate.

Acknowledgements

We are greatly indebted to our technical collaborators and to the funding agencies for their support in building and operating the DELPHI detector, and to the members of the CERN-SL Division for the excellent performance of the LEP collider.

References

[1] CUSB Collaboration, K. Han et al., Phys. Rev. Lett. **55** (1985) 1
[2] CUSB 2 Collaboration, J. Lee-Franzini et al., Phys. Rev. Lett. **65** (1990) 24 /newline
CUSB 2 Collaboration, Q.W. Wu et al., Phys. Lett. **B273** (1991) 177
[3] CLEO 2 Collaboration, D.S. Akerib et al., Phys. Rev. Lett. **67** (1991) 13
[4] L3 Collaboration, M. Acciarri et al., Phys. Lett. **B345** (1995) 589
[5] Particle Data Group, Phys. Rev. D **50** (1994)
[6] N. Isgur, M.B. Wise, Phys. Lett. B 232 (1989) 113;
M.B. Wise, Procs. XVI International Symposium on Lepton and Photon Interactions, Ithaca, New York, 1993, Ed. P. Drell, D. Rubin, p. 253.
[7] DELPHI Collaboration, P. Aarnio et al., Nucl. Instr. Meth. **A303** (1991) 233-276
[8] DELSIM User's Guide, DELPHI 89-15 PROG 130, CERN, February 1989
DELSIM Reference Manual, DELPHI 89-68 PROG 143, CERN, September 1989
[9] T. Sjöstrand, Comp. Phys. Comm. **82** (1994) 74
[10] W. de Boer, H. Fürstenau, *Comparison of DELPHI data with QCD models*, DELPHI Note 91-75 Phys 129;
K. Hamacher, M. Weierstall, *The next Round of Hadronic Generator Tuning heavily based on Identified Particle Data*, Wuppertal Univ. report WU B 95 07
[11] DELPHI Collaboration, P. Abreu et al., Z. Phys. **C 54** (1992) 55
[12] ALEPH Collaboration, D. Buskulic et al., Phys. Lett. B **313** (1993) 535-548
DELPHI Collaboration, P. Abreu et al., CERN-PPE/94-131 (1994)
[13] G. Marchesini et al., Comp. Phys. Comm. **67** (1992) 465
[14] M. Feindt, O. Podobrin, M. Wielers, *Measurement of the Inclusive π^0 Cross Section in Z Decays*, DELPHI Note 94-81 Phys 398.
[15] S. Plaszczynski, LAL-94-17, May 1994.
[16] OPAL Collaboration, R. Akers et al., *Observations of $\pi - B$ charge-flavor correlations and resonant $B\pi$ and BK production*, CERN-PPE/94-206 (1994)
[17] DELPHI Collaboration, P. Abreu et al., Phys. Lett. **B345** (1995) 598
[18] V. Blobel, *Unfolding in High Energy Physics*, Procs. CERN School of Computing, Aiguablava (Spain), Sep. 1984. CERN, Geneva, 1985, p.88.
[19] DELPHI Collaboration, P. Abreu et al., *Measurement of $\Gamma_{b\bar{b}}/\Gamma_{had}$ using Impact Parameter Measurements and Lepton Identification*, CERN-PPE/95-08 (1995)

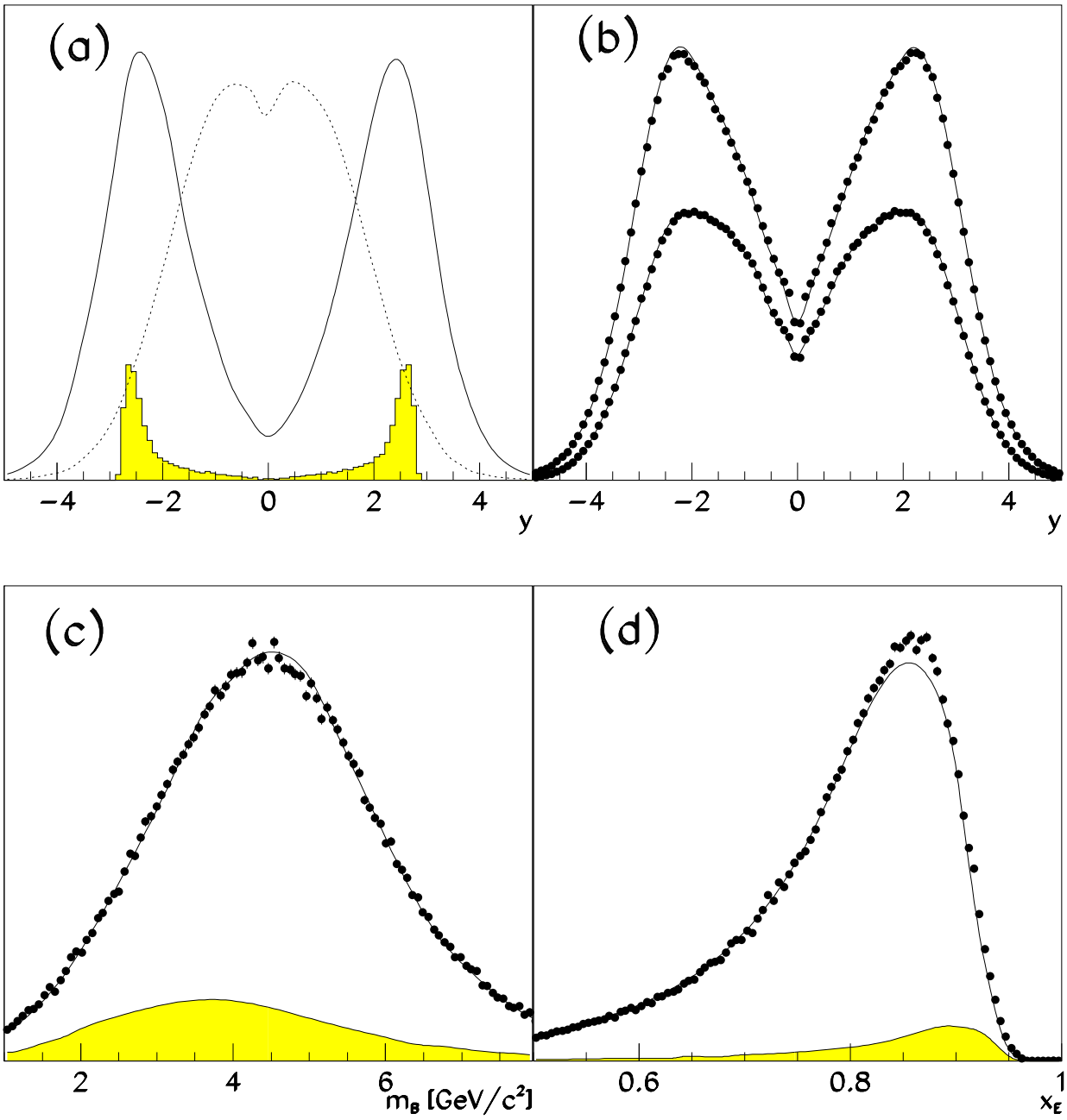

Figure 1: (a) Rapidity distributions for B mesons (shaded area), particles stemming from B decay (solid curve) and particles from fragmentation (dotted curve) in $b\bar{b}$ events as expected from the JETSET 7.4 model.
(b) Comparison between the rapidity distributions of all particles (upper curves) and charged particles (lower curves) in data (points) and Monte Carlo simulation (lines).
(c) Reconstructed B mass spectrum for data (points) and simulation (solid line).
(d) Corrected fractional B energy spectrum for data (points) and simulation (solid line).
The shaded area in (c) and (d) corresponds to the background due to non-$b\bar{b}$ events.

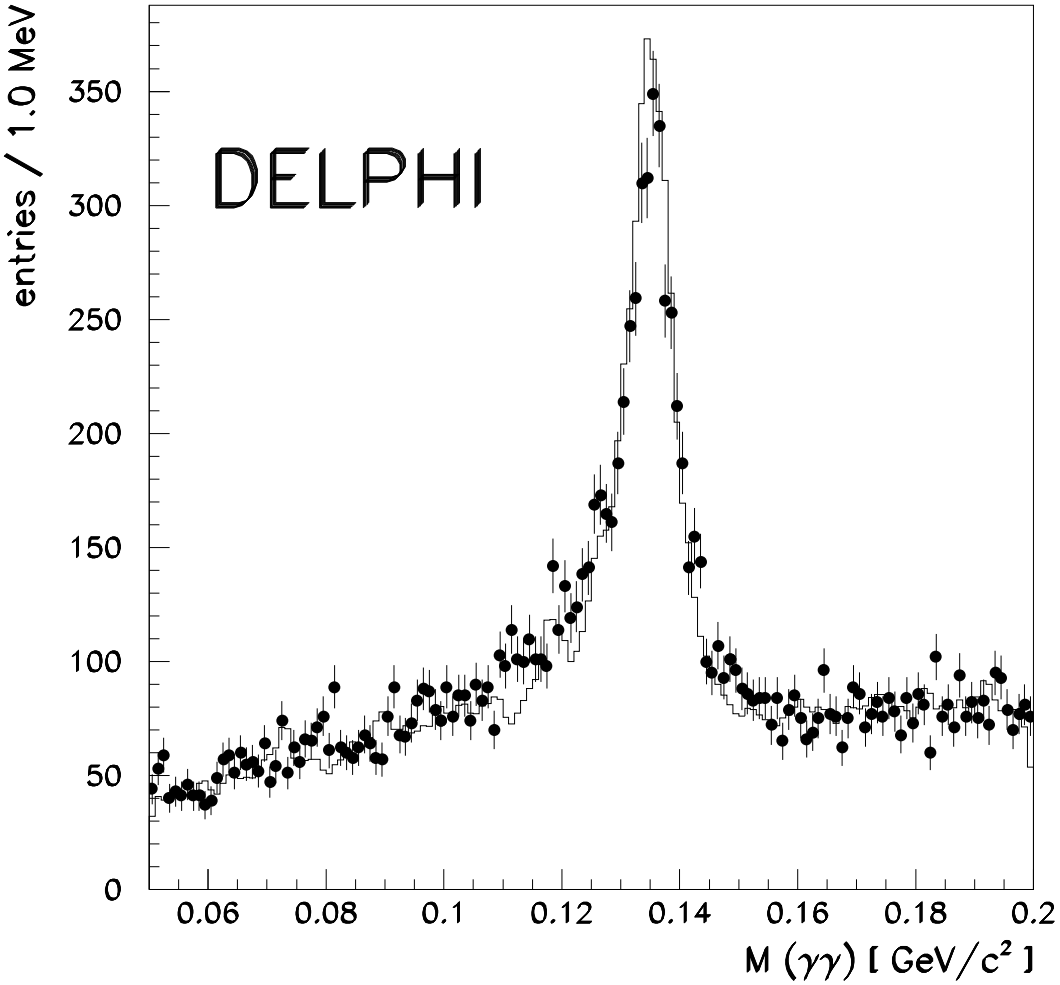

Figure 2: Invariant $\gamma\gamma$ mass from pairs of converted photons. The data (points) are compared with the simulation (solid line).

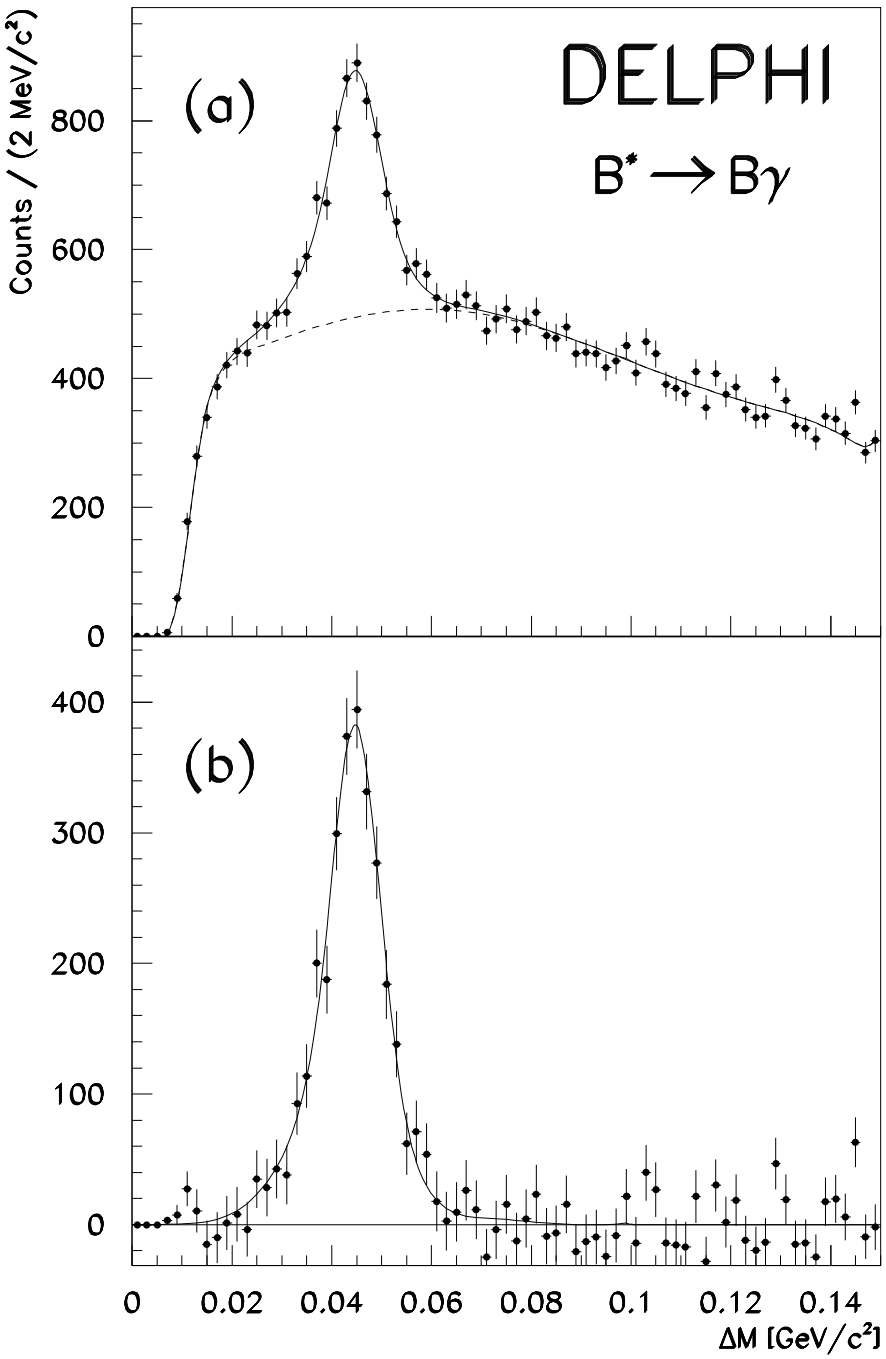

Figure 3: $B\gamma - B$ mass difference distribution. (a) The data are represented by points with the smoothed simulation background and signal shapes superimposed.
(b) The $\Delta M(B^* - B)$ signal after background subtraction. The curve shows the prediction from the simulation with a value of 45.5 MeV/c^2.

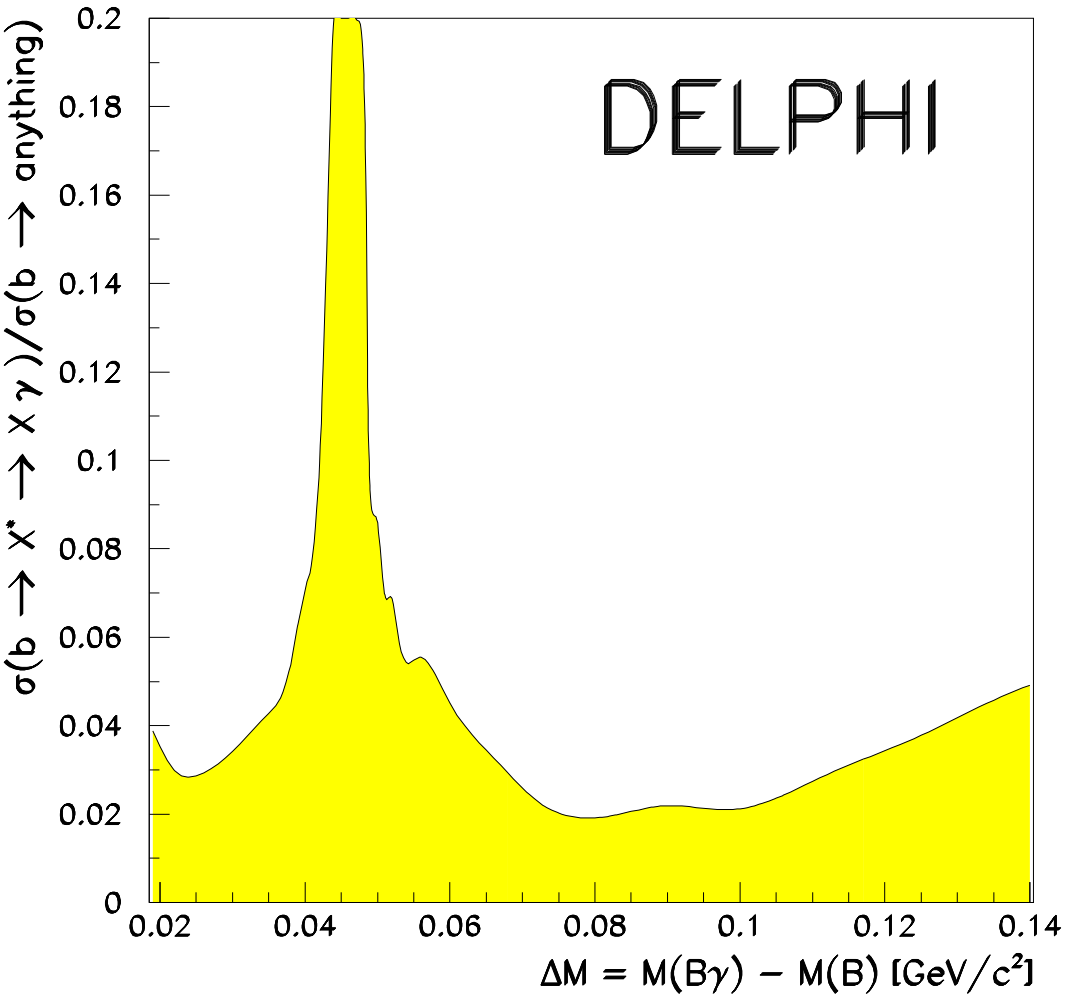

Figure 4: 95% confidence level upper limits on the fraction of b-quarks hadronising into a radiatively decaying hadron $X_b^* \to X_b\gamma$ (excluding B^* production)

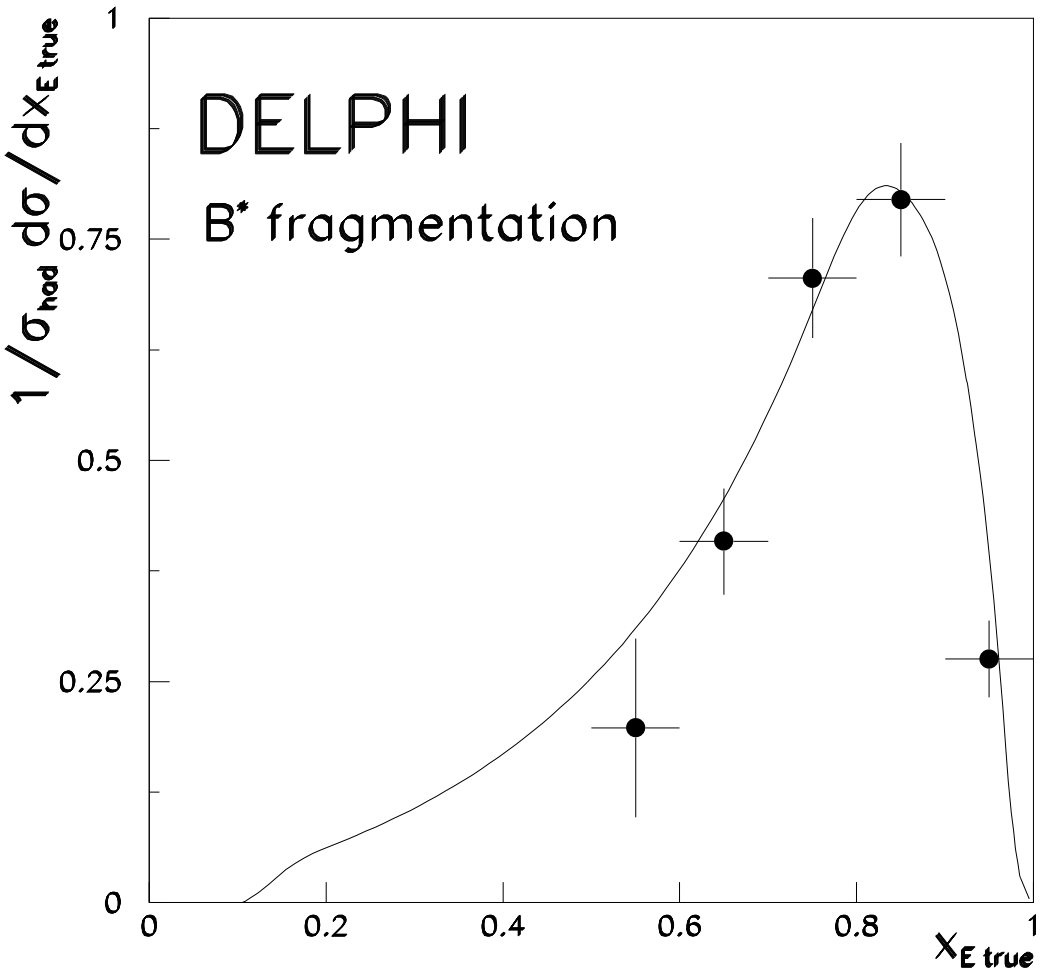

Figure 5: Inclusive B^* cross-section in bins of x_{Etrue}. The points are unfolded data; the curve is the JETSET 7.4 prediction fitted to the data with $\langle x_E \rangle = 0.695$.

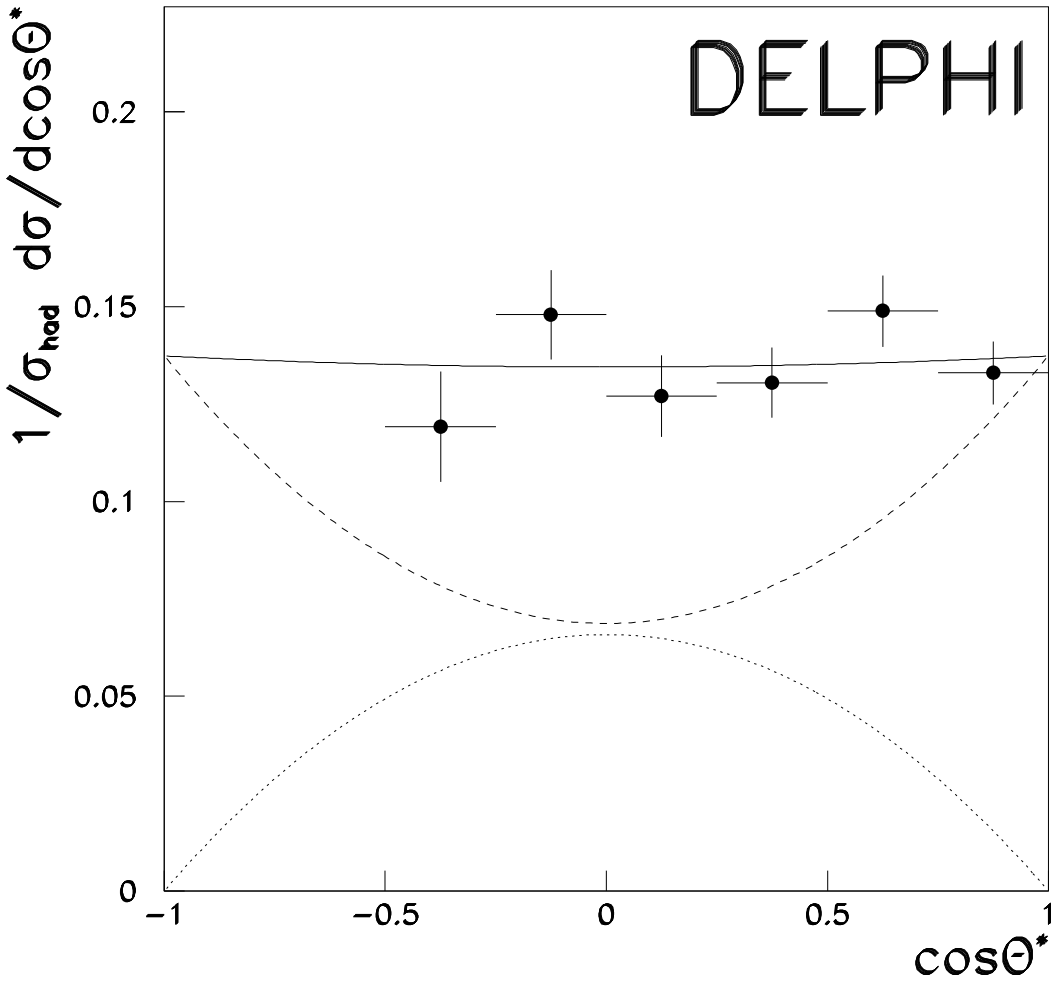

Figure 6: Decay angular distribution for B^* photons in the B^* rest frame. The acceptance corrected data are represented by points. The solid line displays the result of a fit to longitudinal and transverse polarisation contributions. The dashed and dotted curves are the contributions from the transverse and longitudinal states.